journal

J. Am. Ceram. Soc., 79 [8] 2081–90 (1996)

SiAlON Composites Containing Rare-Earth Melilite and Neighboring Phases

Zhen-Kun Huang, Shih-Yu Liu, Anatoly Rosenflanz,* and I-Wei Chen*

Materials Science and Engineering, University of Michigan, Ann Arbor, Michigan 48109-2136

Sintering aids with a formulation of rare-earth (R) melilite solid solution M′(R) have been introduced to several SiAlON composites to obtain high-density bodies by pressureless and gas-pressure sintering. These compositions include ones along the Si_3N_4–R_2O_3:9AlN line, which contain no Al_2O_3 and are known to have excellent strength but very poor sinterability. Phase analysis and property (hardness, toughness, strength, and oxidation resistance) measurements reveal a complex set of structure–property–processing relationships that are composition-dependent. Of the most importance is the Al—O content in various phases, which is dictated by the starting composition as well as Al—O solubility in M′(R). This influences the sinterability, strength, and phase assemblage through the compositions of the intermediate liquid and the final β′-SiAlON. La_2O_3 is further established as an effective sintering aid that does not affect the equilibrium phase assemblage. Overall, M′(R) and La_2O_3 show promise as SiAlON sintering aids that allow high density to be achieved without compromising intrinsic mechanical and thermal properties.

I. Introduction

RARE-EARTH (R) melilite M(R) $R_2O_3{\cdot}Si_3N_4$ and its solid solution M′(R) $R_2O_3{\cdot}Si_{3-x}Al_xO_xN_{4-x}$ have been widely reported as a second phase in SiAlON that contains rare-earth oxides as sintering additives.[1–11] Their occurrence is particularly common in α′-SiAlON, presumably because of the generally higher content of rare-earth oxide required for its sintering. The tendency for forming melilite is most pronounced for lighter rare-earth elements, such as neodymium and samarium but excluding lanthanum. This is due to the affinity of (strongly basic) Nd_2O_3 and Sm_2O_3 to (strongly acidic) Si_3N_4, as predicted by the acid–base theory.[10,11] More broadly speaking, we have demonstrated in the preceding paper[12] that M(R)/M′(R) are compatible with α′- and β′-SiAlON as well as 12H/21R polytypoids. Therefore, it should be possible to obtain various SiAlON composites containing M(R)/M′(R) in the equilibrium phase assemblage. The intent of this paper is to explore the potential of a number of representative SiAlON–melilite composites as structural ceramics by documenting their sinterability, mechanical properties, and oxidation resistance.

Sintering of SiAlON with sintering aids in a melilite formulation entails somewhat different considerations from that with other sintering aids. Most sintering aids are formulated as oxides or their compounds, such as $R_3Al_5O_{12}$, $R_2Si_2O_7$, and $R_5(SiO_4)_3N$; however, melilite is a nitrogen-rich compound. According to the phase diagram of R-Si-(Al/O)-N, a liquid region exists at high temperature, separating the Si_3N_4 corner and the plane of additive oxides and their compounds. In contrast, there is no liquid region between M(R)/M′(R) and the Si_3N_4 corner. Although some liquid does form during initial heating because of the ternary eutectic of SiO_2, Al_2O_3, and R_2O_3, the liquid should be consumed largely by Si_3N_4 to form M(R)/M′(R), if the overall composition is formulated as a SiAlON–M(R)/M′(R) assemblage. This sequence of reactions, indeed, has been verified in our previous work.[10,11] Thus, sintering of the latter composition is relatively difficult at the intermediate temperature for lack of liquid, but it should improve drastically once the melting point of M(R)/M′(R), between ~1700° and 1800°C, is exceeded. Indeed, the lack of liquid at the intermediate temperature could be advantageous, because it reduces the possibility of melt evaporation and massive powder relocation. These advantages have been noted in our preliminary work and Ref. 9.

Guided by the above considerations, we have chosen several representative phase assemblages to explore the feasibility of using M(R)/M′(R) as a sintering aid. The three major groups chosen, schematically shown in Fig. 1, are α′–β′–M′, α′/β′–polytypoid–M′, and (β-α′)–M′. In the above, the first two groups contain various amounts of α′- and β′-SiAlON, which are known to provide composites of contrasting microstructures and properties. The last group incorporates the β-α′ composition, which lies on the α′ plane along the Si_3N_4–R_2O_3:9AlN line and is known to have excellent strength but very poor sinterability.[13,14] Our work shows that, with M(R)/M′(R) as sintering aids, all of these phase assemblages can be sintered to high density without compromise to their intrinsic properties.

II. Experimental Procedures

Compositions of powder mixtures and their nominal phase assemblage investigated in this work are listed in Table I for later reference. For compositions 8–12, the amount of Al_2O_3 listed in Table I is entirely from the residual oxygen in the AlN powders. For compositions 9–12, an additional 2 wt% La_2O_3 is included as a sintering aid. (Lanthanum does not enter either α′- or β′-SiAlON.) The nominal compositions of α′, β′, M′, and 21R used to compute the nominal phase assemblage were fixed at $R_{0.37}Si_{9.6}Al_{2.4}O_{1.29}N_{14.71}$, $Si_{5.23}Al_{0.77}O_{0.77}N_{7.23}$, $R_2Si_2AlO_4N_3$, and $SiAl_6O_2N_6$ and are the same as those listed in Table I in the previous paper.[12] The nominal composition of β-α′ (in compositions 8–12) is $R_{0.1}Si_{11.55}Al_{0.45}O_{0.15}N_{15.85}$. It lies on the Si_3N_4–R_2O_3:9AlN line and has an approximate phase assemblage of 70% β, with the remaining 30% being α′-SiAlON of the $R_{0.3}Si_{10.65}Al_{1.35}O_{0.45}N_{15.55}$ composition. This latter composition has been studied extensively by Ukyo *et al.*[13] and by Sheu[14] to explore its excellent strength at both room temperature and 1400°C.

The starting powders used in this work were identical to those used in the previous paper.[12] The powder mixtures were attrition milled in isopropyl alcohol for 2 h, using silicon nitride (Si_3N_4) milling medium and Teflon™-coated (DuPont, Wilmington, DE) containers. After milling, the powder mixtures were dried, sifted, isostatically pressed under 300 MPa, then placed in a boron nitride (BN) crucible with packing powders

G. L. Messing—contributing editor

Manuscript No. 192317. Received September 20, 1995; approved February 5, 1996.
Supported by the Air Force Office for Scientific Research under Grant No. AFOSR-F49620-95-1-0119.
Presented at the 97th Annual Meeting of the American Ceramic Society, Cincinnati, OH, May 1995 (Paper No. SXIII-56-95).
*Member, American Ceramic Society.

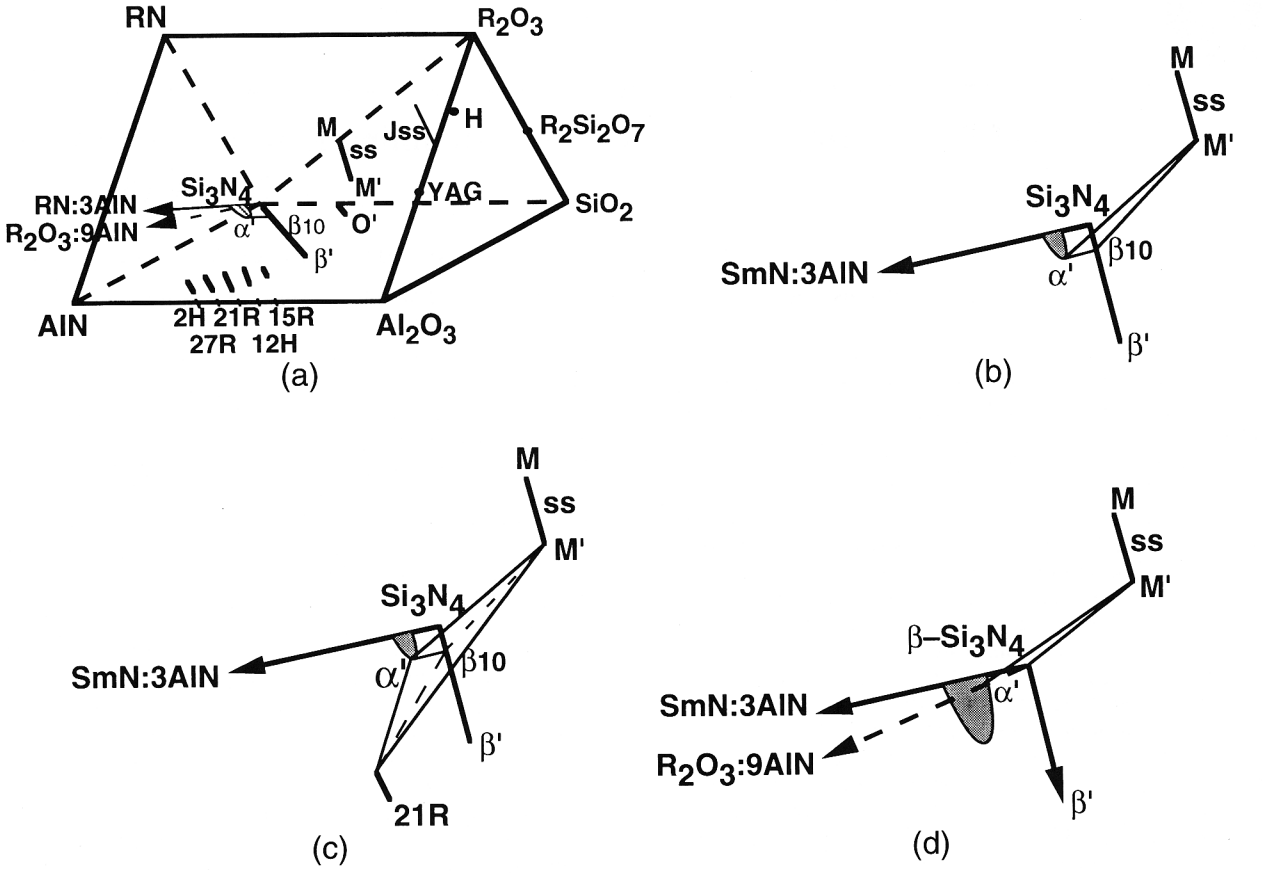

Fig. 1. Composition regions of M′(R)-containing SiAlON composites: (a) R-Si-(Al/O)-N (R = Nd, Sm, Gd, or Yb) system, (b) β′–α′–M′ region, (c) β′/α′–21R–M′ region, and (d) β–α′–M′ (Al_2O_3-free) region.

made of silicon nitride and boron nitride. Sintering was conducted in a graphite furnace, backfilled with 1 atm N_2 at the desired temperature, typically for 2 h. After sintering, the power was turned off and the furnace allowed to cool. A typical cooling rate of 37°C/min was found from 1800° to 1200°C. For some compositions, gas-pressure sintering (GPS) using a nitrogen gas overpressure ranging from 0.3 to 2 MPa also was performed. (The detailed schedule will be described later.) A typical cooling rate of 45°C/min was found from 1950° to 1200°C. Lastly, some runs of hot pressing (HP) were used for compositions 8–12 to provide a reference to the GPS specimens. They were conducted at 1780°C for 1.5 h and followed by furnace cooling. To crystallize the liquid phase and obtain M′, some samples were annealed further at 1550°C for 24 h after sintering. According to Cheng *et al.*,[9] M′ is stable between 1400° and 1600°C, which justifies the above heat treatment for the intended purpose of completely crystallizing M′.

Densified specimens were ground to remove 0.5 mm from the surfaces before density measurement and phase analysis. Density was measured by the Archimedean method using water, and the phase analysis was performed using X-ray diffraction (XRD). For lattice parameter determination, coarse silicon powders were used as an internal standard. Additional compositional analysis also was performed using a microprobe. The above procedures were similar to those described in the companion paper.[12] Microstructural examination was performed in a scanning electron microscope (SEM) using polished specimens etched by plasma.

Bend bars with dimensions 1 mm × 3 mm × 20 mm were obtained from densified specimens. For hot-pressed specimens, the long axis of the specimen lies on the hot-pressing plane and the tensile surface lies normal to the hot-pressing plane. The surfaces of the specimens were finely ground along the long axis, then polished using a 6 μm diamond paste to obtain a good finish. For strength measurements, tests were conducted in N_2 using a tungsten-mesh resistance furnace in a three-point bending configuration with a total span between outer supports at 13 mm. Vicker indentation at 10 kg was used to obtain hardness and effect indentation cracking. The lengths of the four cracks emanating from four corners of each indent were measured, and the indentation toughness was computed using the formula of $K_{IC} = 0.004958(E/H)^{0.5}P/C^{1.5}$ (MPa·m$^{1/2}$), with the appropriate parameters.[15] (E = 300 GPa; H is hardness in MPa, P load in kg, and C the half-length of two diagonal cracks.)

Oxidation experiments using polished samples were performed in air in an alumina tube furnace. Weight gains of samples were measured after exposure at different temperatures up to 1400°C for different times up to 120 h.

III. Results and Discussion

(1) *Sinterability and Phase Compositions*

(A) Samarium-Containing α′–β′–M′ Region: Measured densities with compositions in this series are listed in Table II, along with the results of phase analysis. Most of the specimens could be sintered to high density at 1750°C within 2 h without N_2 overpressure. The composition of 80β′:18α′:2M′, which contained the least Sm_2O_3, required a higher temperature (1800°C) to reach the high density. Theoretical densities were not determined because of the polyphase nature of these compositions. However, they are expected to be very close to the as-sintered values in Table II, judging from the physical appearance of the polished surfaces of the specimens and their relatively high strengths described later in Section (III)(2)(*C*).

The results of phase analysis shown in Table II confirmed the intended phase assemblages. In the as-sintered state, the majority phase was either α′ or β′, with a small number of minority phases. Annealing at 1550°C for 24 h typically caused

Table I. Compositions of Powder Mixtures

Composition number	Designated phase assemblages (wt%)	Composition (wt%)				
		Si_3N_4	AlN	Al_2O_3	R_2O_3	La_2O_3
	α′–β′–M′(R) region					
1	80α′:10β′:10M′(Sm)	69.04	12.18	3.28	15.50	
2	80α′:15β′:5M′(Sm)	72.41	12.24	3.41	11.94	
3	80β′:10α′:10M′(Sm)	78.38	4.83	8.63	8.17	
4	80β′:15α′:5M′(Sm)	81.08	5.41	8.39	5.13	
5	80β′:18α′:2M′(Sm)	82.70	5.76	8.24	3.31	
	SiAlON–polytypoid–M′(R) region					
6	80β′:10(21R):10M′(Sm)	72.60	9.64	10.65	7.12	
7	80α′:10(21R):10M′(Sm)	61.93	18.04	4.53	15.50	
	Al_2O_3-free (β-α′)–M′(R) region					
8	95β–α′(x = 0.1):5M′(Sm)	90.04	3.18	0.35	6.44	
	Al_2O_3-free (β-α′)–M′(R)–2La region					
9	93(β-α′)(x = 0.1):5M′(Nd):2La	88.28	3.13	0.36	6.24	2.00
10	93(β-α′)(x = 0.1):5M′(Sm):2La	88.16	3.12	0.35	6.38	2.00
11	93(β-α′)(x = 0.1):5M′(Gd):2La	88.03	3.11	0.34	6.52	2.00
12	93(β-α′)(x = 0.1):5M′(Yb):2La	87.74	3.10	0.32	6.85	2.00

an increase in the amount of melilite solid solution present, accompanied by a relative decrease in the XRD intensity of the majority phase. XRD further detected a peak shift in the majority phase. In the case of β′ being the majority phase, its lattice parameters decreased, after annealing, which is consistent with a decrease in the Al—O content. A similar trend was seen in α′, whose lattice parameters also decreased after annealing. Although the composition of α′ cannot be determined uniquely from lattice parameters alone, which depend on more than one component in the composition, microprobe analysis in the companion paper[12] established that the "equilibrium" α′ composition after annealing was m = 1.11 and n = 0.92. It also established the equilibrium compositions for β′ to be β_{10} and for M′ to be x = 0.9. These results can be interpreted as indicating α′/β′ dissolution and M′ precipitation during annealing, with the remaining α′/β′ undergoing solute redistribution, thus providing the rejected cations (aluminum and samarium) that entered M′.

Microstructures of these compositions in the as-sintered state were examined, and they largely confirmed the expected phase assemblages. For example, in the case of 80α′:10β′:10M′, a fine-grained α′ matrix was seen in the as-sintered specimen with dispersed β′ rods and pockets of M′ liquid; this is shown in Fig. 2(a). The microstructure of 80β′:10α′:10M′, on the other hand, contained a matrix of acicular β′ grains of various sizes with the other phases only inconspicuously shown (Fig. 2(b)). It is interesting to note that, in Fig. 2(a), M′ liquid (the white region due to Z (atomic number) contrast of the samarium-rich composition) occupies large interstices between α′ grains. In contrast, in Fig. 2(b), pockets of M′ liquid are not visible, presumably because M′ liquid is now spread between β′ grains and occupies only very small interstices. After annealing, we found that the α′-rich composition contained M′ particles of somewhat smaller sizes than before (compare Fig. 2(c) with Fig. 2(a)). However, the β′-rich composition also contained many large M′ pockets (compare Fig. 2(d) with Fig. 2(b)). Using quantitative microscopy, we have further estimated the volume fraction of the white region to be ~9% in Fig. 2(a), 12% in Fig. 2(c), and 8% in Fig. 2(d). These values are essentially consistent with the expected phase assemblage of M′ and its liquid. Thus, the above difference in the microstructure probably was not due to a large difference in the actual liquid amount of oxides at the sintering temperature, but rather due to different temperature-dependent wetting characteristics of the transient liquid with the matrix phases similar to that recently reported by our group.[10] Poorer wetting characteristics then could lead to large M′ liquid pockets in the α′-rich composition to be bordered by phase boundaries of α′–M′, which are concave in shape, in contrast to better wetting characteristics in the β′-rich composition, which allow the liquid to spread evenly between grains.

Comparing the above micrographs with the XRD results in Table II, we find that the crystallization of M′ during annealing can be attributed to the liquid that remained after sintering. This is reflected in a very substantial increase in the M′ intensity in XRD in all of the annealed samples, even though the increase in the area fraction of the white regions in the corresponding micrographs is only modest. (We, obviously, have assumed that there is, in Fig. 2(b), a substantial amount of the liquid region that is distributed too finely to be measured accurately by quantitative microscopy in our work.) This also implies that there cannot be any significant conversion of α′-SiAlON to β′-SiAlON, which must be accompanied by an attendant formation of additional M′ crystals or liquid. The latter recently have been reported by several investigators.[16,17]

The lack of such conversion also is consistent with the micrographs of Figs. 2(a) and (c), which do not reveal a significant increase of acicular β′ grains upon annealing. Such conversion

Table II. Sintering Conditions, Phase Assemblages, and Properties of α′–β′–M′(Sm) Composites

Composition number*	Phase assemblages (wt%)	Sintering conditions (°C/h)	Density (Mg/m^3)	Phase analysis†			Lattice parameter (Å)		Hardness, H_v (GPa)	Toughness, K_{1C} ($MPa \cdot m^{1/2}$)
				α′	β′	M′	a	c		
1	80α′:10β′:10M′	1750/2	3.501	vs	vw	vw	7.846	5.716 (α′)	18.5	4.1
		+1550/24	3.498	s	vw	ms	7.835	5.711 (α′)		
2	80α′:15β′:5M′	1750/2	3.416	vs					18.2	4.8
		+1550/24	3.424	s	w	ms				
3	80β′:10α′:10M′	1750/2	3.335	vw	vs	vw	7.645	2.932 (β_{15})	15.3	5.0
		+1550/24	3.304	vw	s	ms	7.633	2.922 (β_{10})		
4	80β′:15α′:5M′	1750/2	3.278	vw	vs	vw			15.7	5.4
		+1550/24	3.269	vw	s	ms				
5	80β′:18α′:2M′	1800/2	3.238	vw	vs		7.637	2.930 (β_{12})	16.9	6.2
		+1550/24	3.236	vw	vs					

*See Table I. †X-ray intensity: vs > s > ms > w > vw.

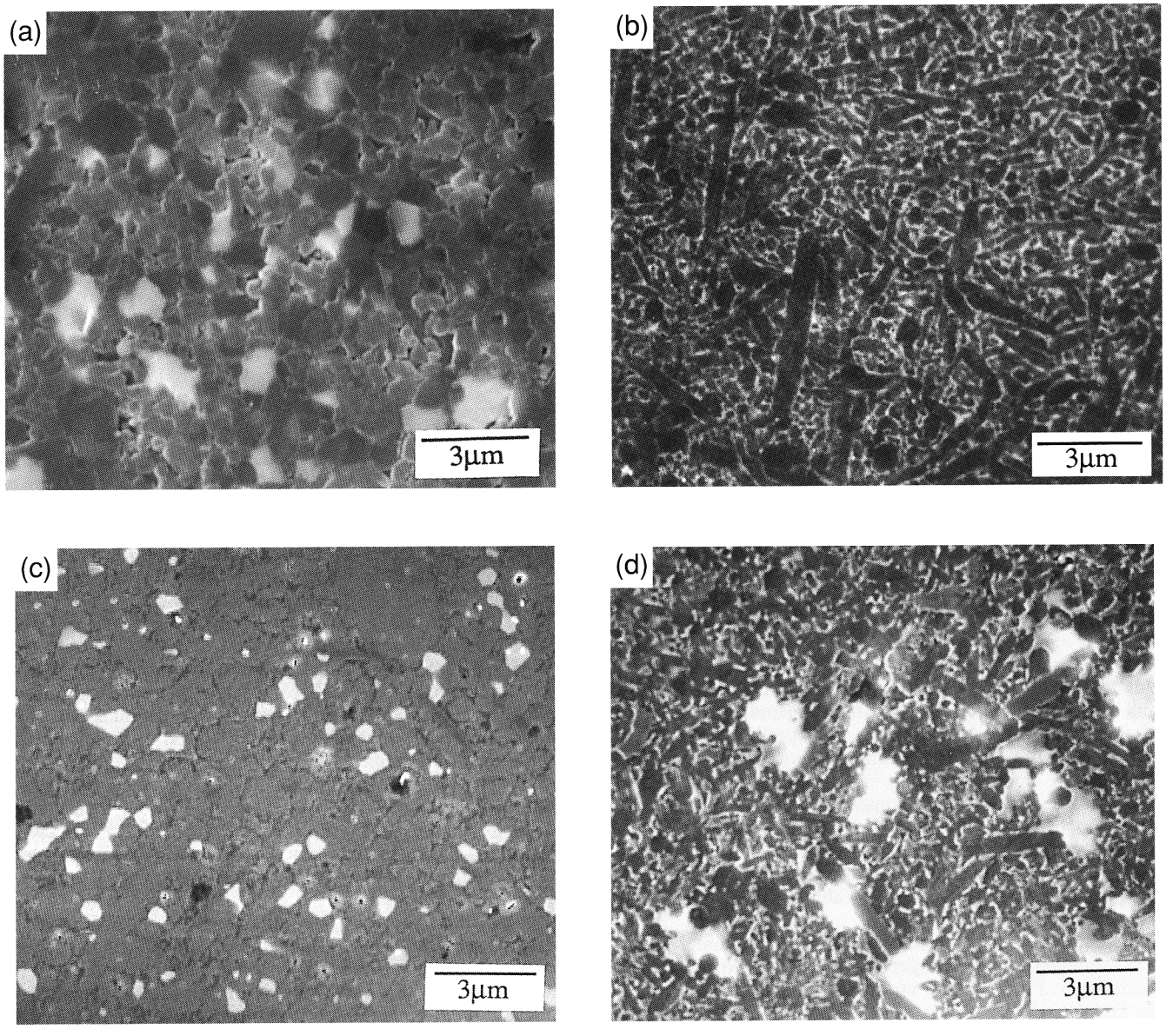

Fig. 2. Microstructures of (a) 80α′:10β′:10M′(Sm) and (b) 80β′:10α′:10M′(Sm) compositions sintered at 1750°C for 2 h; (c) and (d) have the same composition as (a) and (b), respectively, but were annealed additionally at 1550°C for 24 h.

could have occurred to some extent in the β′-rich composition, although neither our data nor those in the literature are sufficient to substantiate this claim, considering the minority amount of α′ phase present in the as-sintered samples, which makes α′-phase quantitative analysis by XRD much more challenging.

(B) Samarium-Containing α′/β′–21R′–M′ Region: Specimens with compositions containing 10% 21R, 10% M′, and 80% α′/β′ could be sintered to high density at 1750°C after 2 h, without N_2 overpressure. The results on sintering and phase analysis are summarized in Table III. The observed phase assemblages essentially agreed with those intended, with the exception that the polytypoid that formed was 12H in the case of the β′-rich composition and 21R for the α′-rich composition. This preference of 12H (Al_2O_3-rich) over 21R (AlN-rich) in the case of the β′-rich specimen seems reasonable considering the higher Al_2O_3 content versus AlN in the starting composition (see Table I). Once again, annealing caused the amount of crystalline M′ to increase, with some attendant decrease in the lattice parameters of the α′- and β′-SiAlONs. Thus, phase reactions very similar to those described in Section (III)(*1*)(*A*) must have occurred in this series during annealing. Comparing Table III with Table II, however, we note that the composition of β′ in 80β′:10(21R):10M′ is richer in Al—O than that of β′ in 80β′:10α′:10M′. This is again reasonable, considering the higher Al_2O_3 content in the former composition (see Table I).

Microstructures of these specimens in the as-sintered state were quite similar to those shown previously in Fig. 2. For the α′-rich composition, shown in Fig. 3(a), a fine-grain α′ matrix with dispersed elongated polytypoid grains can be discerned. Also, large pockets of M′ once again have accumulated at grain interstices. The microstructure of the β′-rich composition shown in Fig. 3(b) is similar to that of Fig. 2(b), containing acicular grains that are either β′ or 12H, without an obvious accumulation of M′ liquid in large pockets. The microstructures after annealing are shown in Figs. 3(c) and (d). No significant change in the matrix is seen in either case. As before, some accumulation of large M′ crystals is evident after annealing in the β′-rich composition, but the reaction in Fig. 3(d) has proceeded to a much-lesser extent than that in Fig. 2(d), indicating a slower crystallization in the AlN-rich composition. Quantitative microscopy found that the M′ liquid/crystallites constitute 10% of the composition in Fig. 3(a), 13% in Fig. 3(b), and 2% in Fig. 3(d). Again, we did not detect a massive conversion of α′ to β′ in the α′-rich composition.

(C) Al_2O_3-Free (β-α′)–M′ Region: This series was prepared without using Al_2O_3 in the starting composition. (However, some Al_2O_3 did enter through the residual oxygen in the

Table III. Sintering Conditions, Phase Assemblages, and Properties of SiAlON–Polytypoid–M′(Sm) Composites

Composition number*	Phase assemblages (wt%)	Sintering conditions (°C/h)	Density (Mg/m^3)	Phase analysis†				Lattice parameter (Å)		Hardness, H_v (GPa)	Toughness, K_{IC} ($MPa \cdot m^{1/2}$)
				α′	β′	M′	P	*a*	*c*		
6	80β′:10(21R):10M′	1750/2	3.324		vs		w (12H)	7.653	2.937 (β′18)	15.4	7.3
		+1550/24	3.321		s	w	w (12H)	7.649	2.936 (β′17)		
								3.040	32.87 (12H)		
7	80α′:10(21R):10M′	1750/2	3.516	vs		w	w (21R)	7.846	5.719 (α′)	18.5	5.8
		+1550/24	3.523	s		m	w (21R)	7.837	5.703 (α′)		
								3.044	57.13 (21R)		

*See Table I. †X-ray intensity: vs > s > m > w. P is polytypoid.

AlN powders.) The overall phase assemblage was chosen to contain 95% SiAlON, of which the β:α′ ratio was 7:3. The remaining 5% was samarium-containing M′. Although specimens of the above composition were quite difficult to sinter at temperatures up to 1800°C, high density could be achieved by GPS using the following schedule: 1 h at 1800°C with 0.3 MPa N_2, followed by 3 h at 1950°C with 2 MPa N_2. Also, the addition of 2% La_2O_3 facilitated sintering considerably. As a result, GPS at 1900°C for 3 h (2 MPa N_2) routinely yielded high densities. This was confirmed not only for samarium-containing specimens but also for other specimens of a similar composition yet with different rare-earth elements (i.e., Nd, Gd, and Yb in place of Sm). To ascertain these results, we also have hot pressed specimens of identical compositions at 1780°C for 1.5 h. The density data and the phase analysis of these specimens are shown in Tables IV and V. In all cases, the density reached after GPS was >99.5% of the hot-pressed specimens.

The beneficial effect of La_2O_3 addition on sintering has been noted before in our work.[18] Among rare-earth oxides, La_2O_3 is expected to give the lowest viscosity and the lowest Young's

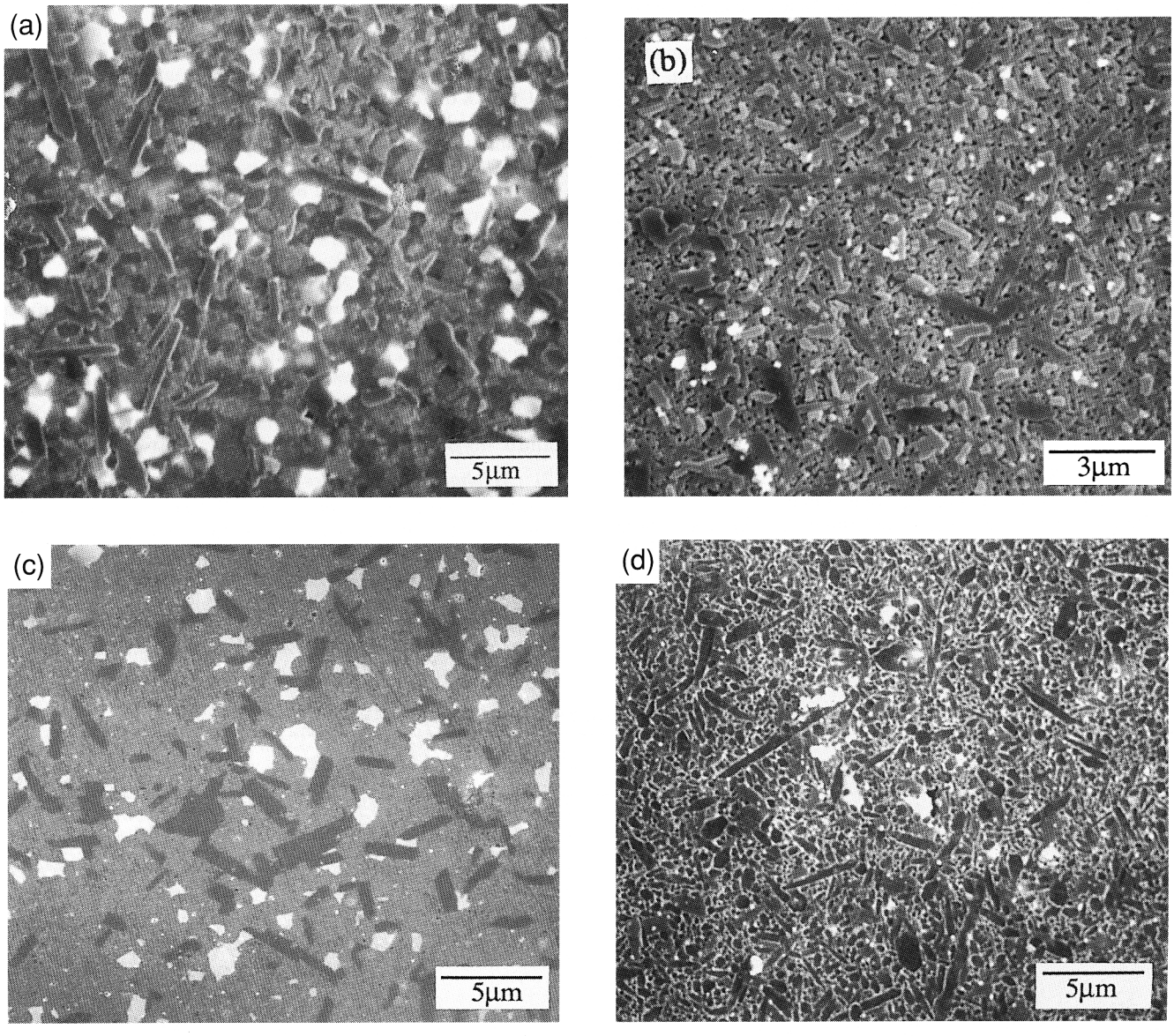

Fig. 3. Microstructures of (a) 80α′:10(21R):10M′(Sm) and (b) 80β′:10(21R):10M′(Sm) compositions sintered at 1750°C for 2 h; (c) and (d) have the same composition as (a) and (b), respectively, but were annealed additionally at 1550°C for 24 h.

Table IV. Processing Conditions, Phase Assemblages, and Properties of an Al_2O_3-Free (β′-α′)–M′(Sm) Composite (Composition 8 in Table I)

Processing method	Processing conditions (°C/h)	Density (Mg/m^3)	Relative density* (%)	Phase analysis† α′	β′	M′	Lattice parameter (Å) a	c	Hardness H_v (GPa)	Toughness, K_{IC} ($MPa \cdot m^{1.2}$)
Sintering	1800/4	3.160	95.3	w	vs	vw	7.633	2.921 (β9)		
	+1550/24	3.129			vs	w				
GPS	1800/1									
	+1950/3	3.305	99.6	vw	vs	vw	7.630	2.919 (β8)	16.1	7.4
	+1550/24	3.304			vs	m				
HP	1780/1.5	3.317	100	mw	s	w	7.636	2.921 (β10)	17.9	7.8
	+1550/24	3.265		vw	s	mw				

*Relative to the HP samples. †X-ray intensity: vs > s > m > mw > w > vw.

modulus to the glass because of its low field strength that results from the large ionic size.[19] Because lanthanum is too large to enter α′-SiAlON, its main effect probably is limited to the conditioning of the liquid phase during sintering without affecting the final assemblage. This point was verified by comparing the β′ compositions of hot-pressed samarium-containing specimens in Tables IV and V. They were all similar to β_9 and essentially indistinguishable, whether lanthanum was present or not.

A systematic comparison of the sinterability and phase composition between compositions containing different rare-earth elements revealed an interesting aspect that is related directly to the different Al—O solubility in different M′(R). Excluding ytterbium, which does not form M′ according to the companion paper,[12] we see from Table V that the gadolinium-containing specimens had the highest relative density, whereas the neodymium-containing specimens had the lowest relative density. This is accompanied by the observation that the Al—O content of β′ in the gadolinium-containing specimens was much higher than that in the neodymium-containing specimens. These observations can be rationalized if we recall that M′(Nd) contains the highest amount of Al—O among all M′(R), whereas M′(Gd) has the lowest amount of Al—O among M′(Nd, Sm, Gd).[12] Thus, it stands to reason that the competition of M′ for Al—O caused the neodymium-containing composition to have a lower Al—O content in the liquid and vice versa for the gadolinium-containing composition. Because a higher Al—O content in the liquid generally is regarded as beneficial for liquid-phase sintering, such reasoning immediately leads to the conclusion of a better sinterability in the gadolinium-containing composition than in the neodymium-containing composition. Similarly, the different Al—O content in the liquid phase leads to a different Al—O content in β′.

Hot-pressured specimens containing M′(R) also were annealed at 1550°C. An increase in the M′ intensity in XRD, indicating crystallization, was observed in all cases except in the ytterbium composition. This parallels our previous observations of M′ crystallization during annealing and is not discussed further here.

Finally, microstructures of these specimens were examined and contain essentially a matrix of acicular β′ grains. For comparison, micrographs of samples prepared by HP and GPS, both containing neodymium or gadolinium and lanthanum, are shown in Fig. 4. The microstructure is obviously finer in the hot-pressed specimen, because of the lower firing temperature and shorter time. However, the main features of the microstructure remain the same under both processing conditions. Moreover, for similarly processed materials in this series, microstructures were almost indistinguishable, regardless of the rare-earth elements used. Lastly, micrographs of GPS samples, after annealing, also are shown in Fig. 4. A few large M′ crystals again can be detected (more in the neodymium composition than the gadolinium composition), but the matrices apparently remain little changed by heat treatment.

The lack of micrographic evidence of massive transformation of α′- to β′-SiAlON, with the attendant formation of M′ liquid/crystallites, in these series of compositions is worth comment. Previously, in Section (III)(*1*)(*A*), we argued that the possibility of such a conversion could be ruled out except perhaps in the β′-rich composition. In the Al_2O_3-free (β-α′)–M′ region, the chosen β-α′ composition ($x = 0.1$) has an approximate phase assemblage of 70% β, with the remaining 30% being α′-SiAlON of the $R_{0.3}Si_{10.65}Al_{1.35}O_{0.45}N_{15.55}$ composition (see Section II). Thus, these samples contain an amount of α′-SiAlON that is a factor of ~3 more than that of the β′-rich samples described in Section (III)(*1*)(*A*). Yet, despite the higher α′ content, the Al_2O_3-free β-rich samples show less M′ formation and little matrix alteration after annealing. Taken together, this seems to suggest that, even in β(β′)-rich samples, very little α′-to-β′ conversion has occurred in our work.

(2) Mechanical Properties

Scoping experiments on the mechanical properties of the SiAlON composites were performed to assess their potential as structural materials. The basic trends revealed by these data reflect the structure–processing–property relations summarized below.

(A) Hardness: Data of hardness have been tabulated in the various tables described above. Hardness values of sintered

Table V. Phase Assemblages and Properties of 93(β-α′)($x = 0.1$):5M′(R):2La_2O_3 Composites

Composition number*	Rare-earth element, R	Process	Phase analysis† β′	α′	M′	Lattice parameter (Å) a	c	Density (Mg/m^3)	Relative density‡ (%)	Hardness, H_v (GPa)	Toughness, K_{IC} ($MPa \cdot m^{1/2}$)
9	Neodymium	GPS	s		tr	7.614	2.913 (β_3)	3.323	99.5	16.1	6.7
		HP	vs	vw	vw	7.617	2.915 (β_4)	3.340	100	18.0	7.7
		+1550°C/4 h	vs	vw	w						
10	Samarium	GPS	vs			7.634	2.920 (β_9)	3.335	99.7	16.2	7.4
		HP	vs	vw	vw	7.632	2.920 (β_9)	3.345	100	17.9	7.8
		+1550°C/4 h	vs	vw	mw						
11	Gadolinium	GPS	vs	tr	tr	7.629	2.919 (β_7)	3.353	100	16.3	6.8
		HP	vs	vw	vw	7.631	2.919 (β_8)	3.354	100	17.9	8.2
		+1550°C/4 h	vs	vw	mw						
12	Ytterbium	GPS	vs	vw		7.613	2.913 (β_3)	3.366	99.6	16.4	7.3
		HP	vs	w		7.632	2.920 (β_9)	3.379	100	16.9	8.2
		+1550°C/4 h	vs	w							

*See Table I. †X-ray intensity: vs > s > mw > w > vw > tr. ‡Relative to hot-pressed samples.

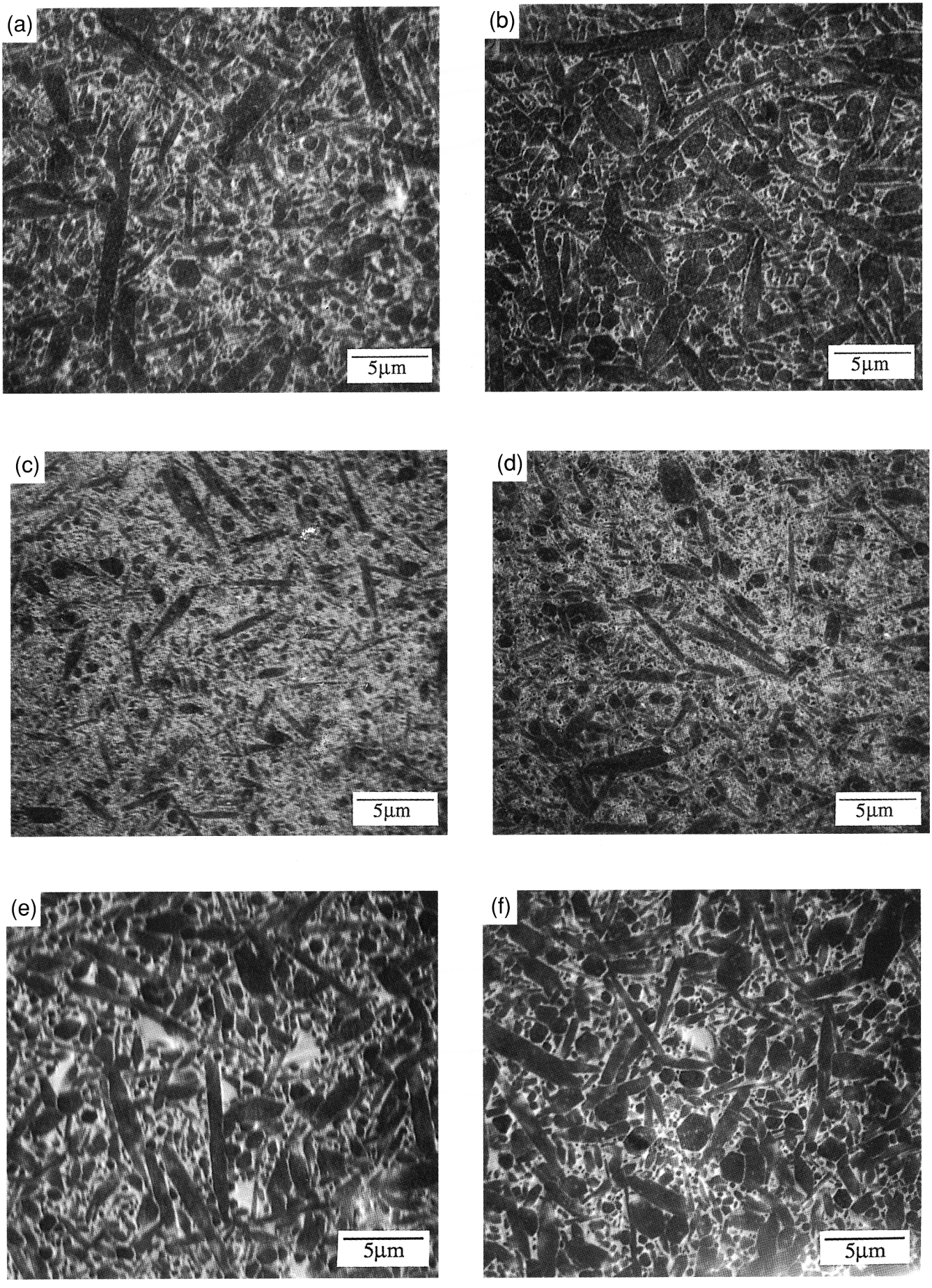

Fig. 4. Microstructure of 93(β-α′):5M′(R):2La composition ((a) R = Nd and (b) R = Gd, both GPS at 1950°C under 2 MPa N_2 for 3 h; (c) R = Nd and (d) R = Gd, both HP at 1780°C for 1.5 h; and (e) R = Nd and (f) R = Gd, both annealed at 1550°C for 24 h after GPS).

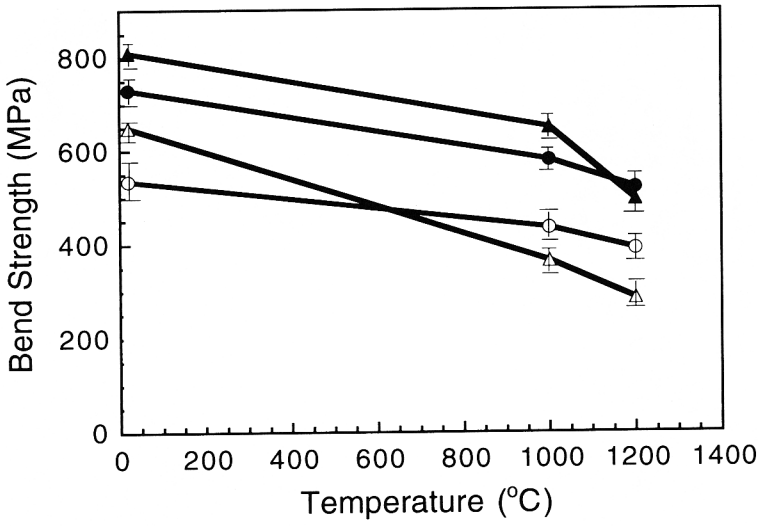

Fig. 5. Bend strength of M′(Sm)-containing SiAlON composites ((○) 80α′:10β′:10M′(Sm), (●) 80β′:10α′:10M′(Sm), (△) 80α′:10(21R):10M′(Sm), and (▲) 80β′:10(21R):10M′(Sm)) at three temperatures.

composites with or without N_2 overpressure fall into two broad bands. For specimens in which α′-SiAlON is the majority phase, their hardness values are ~18 GPa. This compares with the lower values, ~16 GPa, for composites containing mostly β′-SiAlON. This trend is in agreement with the numerous observations reported in the literature.[20,21] It can be attributed to the fact that α-Si_3N_4 is intrinsically harder than β-Si_3N_4 because of the longer Burgers vector for dislocations in the former structure, leading to a higher yield stress for plastic deformation.[22]

Hardness values of the hot-pressed (HP) specimens in the Al_2O_3-free compositions are consistently higher than the ones obtained from the sintered (GPS) specimens. The difference ranges from 0.5 to 2 GPa. Because the relative density difference between these specimens is <0.5%, it is not likely to affect hardness to any appreciable extent. Thus, the hardness contrast is probably due to the finer microstructure of the hot-pressed specimens, which had a lower processing temperature and shorter time. Finer grain sizes have been known to harden polycrystalline materials, including ceramics,[23] because of the disruption of dislocation glide by grain boundaries.

(B) Indentation Toughness: Indentation toughness data have been tabulated above in various tables. Three trends are detected from inspection of these data. First, specimens with a high β′ content have a higher toughness than those with a high α′ content. This is in accord with the current understanding that elongated, rodlike grains of β phase impart toughness by way of grain bridging and pullout in the crack wake.[24] Second, specimens free of Al_2O_3 have significantly higher toughness than those containing Al_2O_3, whether La_2O_3 was used as an additive or not. This holds for samples sintered under N_2 overpressure at higher temperatures and samples hot pressed at lower temperatures. (The latter specimen had a higher toughness most likely due to grain alignment on the hot-pressed plane.) These specimens all had a β′-rich matrix and a much-higher Si_3N_4 content in the starting composition. Comparing them with the other β′-rich specimens, such as 80β′:10α′:10M′ and 80β′:10(21R):10M′, we note that the Al—O content in β′ is much lower in the Al_2O_3-free series. Because the bond strength of β′ decreases with increasing Al—O content, this trend is reasonable and indicates the importance of strong grains in realizing the maximal benefit from the grain bridging/

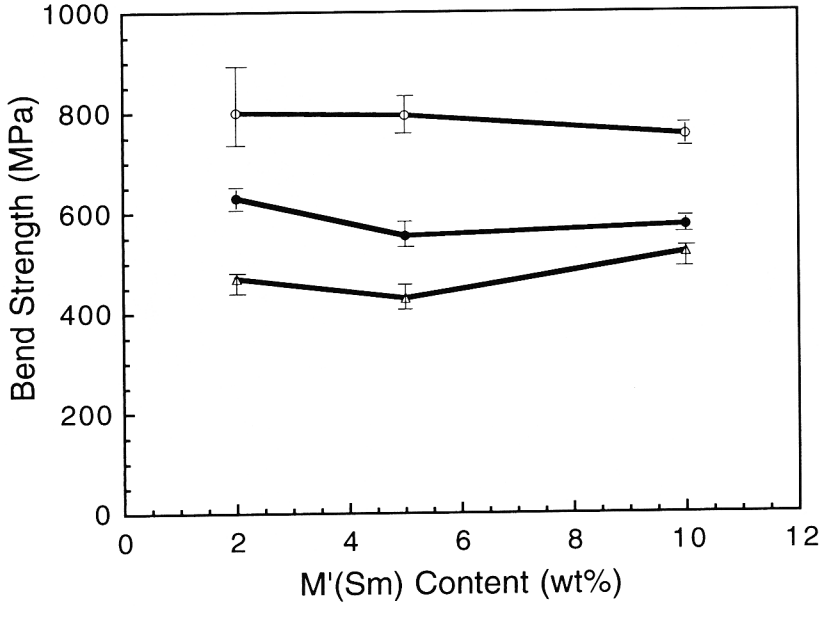

Fig. 6. Bend strength of β′-rich composites at three M′(Sm) contents ((○) room temperature, (●) 1000°C, and (△) 1200°C).

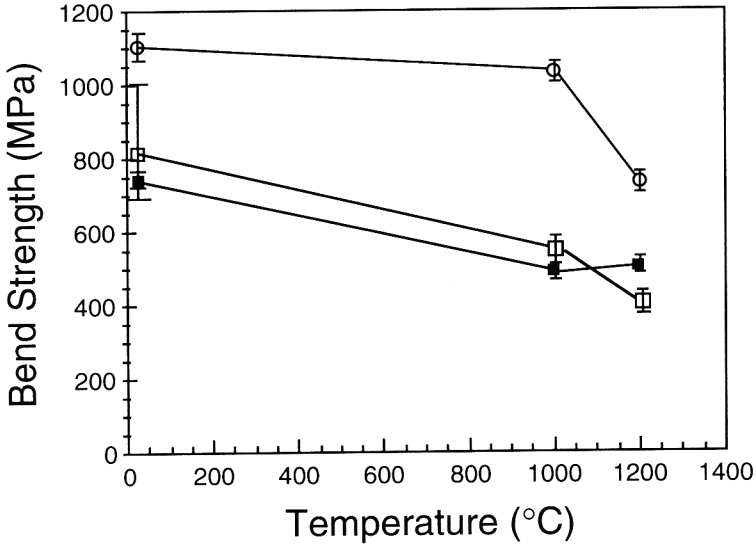

Fig. 7. Bend strength of Al_2O_3-free 95(β-α′):5M′(Sm) composites at three temperatures ((○) 95(β′-α′):5M′ (HP), (□) 95(β′-α′):5M′ (GPS), and (■) annealed).

pullout mechanism. Third, HP specimens have a higher toughness than those sintered by GPS. This could reflect the formation of stronger grains under HP by elimination of crystalline defects in HP samples than in GPS samples.

(C) Bend Strength: Selective data of bend strength as a function of temperature are shown in Figs. 5–8. Figure 5 compares the strength values of composites of various phase assemblages, all containing 10% M′ and sintered at 1750°C without N_2 overpressure. The average strength at room temperature varies from 800 to 550 MPa. The highest strengths were found in samples of the highest content of elongated phases, including both β′-SiAlON and polytypoids. (Thus, 80β′:10(21R):10M′ had a higher strength than 80β′:10α′:10M′ because of the additional contribution of polytypoids, even though the amount of β′ was the same.) Samples rich in α′-SiAlON had lower strength, although 80α′:10(21R):10M′ had a higher strength than 80α′:10β′:10M′, possibly because of the better sinterability of the former, considering the higher amount of additives used. In regard to the high-temperature data, we find the strength at 1200°C increases monotonically with the amount of Si_3N_4 in the starting composition. This correlation suggests a deleterious effect of non-Si_3N_4 additives to the high-temperature strength of SiAlON composites. Lastly, data shown in Fig. 6, for β′-rich β′–α′–M′ compositions containing different amounts of M′, indicate that the average strength is not influenced significantly by the amount of the melilite. However, because the data scatter does decrease substantially, especially at room temperature, with the amount of M′, the true strengths of low-M′ specimens at low temperatures could have been higher but probably were masked by their poorer sinterability, which left a higher flaw population.

Strength data of Al_2O_3-free composites, shown in Figs. 7 and 8, include measurements on both HP and GPS samples. Naturally, hot-pressed samples have higher strengths in nearly all cases. More interestingly, we note that among samples with a La_2O_3 sintering aid (Fig. 8), the neodymium composition had the highest strength after HP but the lowest strength after GPS, whereas the gadolinium composition had the lowest strength after HP but achieved nearly the same strength after GPS. As shown previously in Fig. 4, the microstructure was finer in the HP condition than in the GPS condition. Yet, this difference

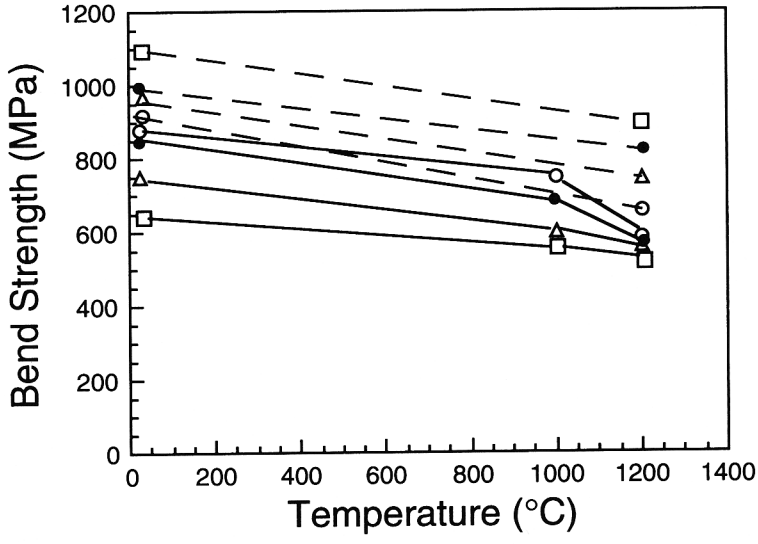

Fig. 8. Bend strength of 95(β-α′):5M′(R):2La composites obtained by (---) HP and (—) GPS ((□) β–α′–M′(Nd), (△) β–α′–M′(Sm), (○) β–α′–M′(Gd), and (●) β–α′–M′(Yb)).

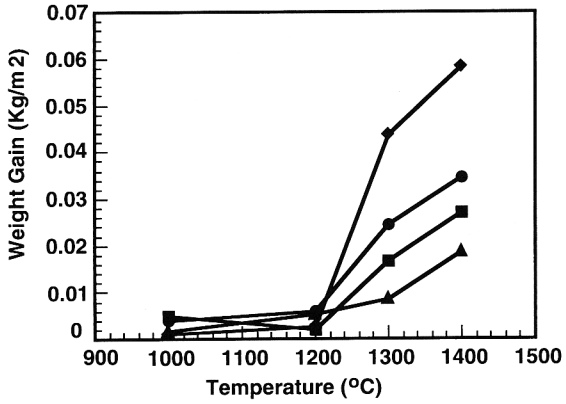

Fig. 9. Weight gain of α′–β′–M′(Sm) composites in air after 20 h ((◆) 80α′:10β′:10M′, (●) 80β′:10α′:10M′, (■) 80α′:15β′:5M′, and (▲) 80β′:15α′:5M′).

in microstructure did not lead to different strength for the gadolinium-containing specimen. Therefore, microstructure probably is not the main reason for the different strengths observed, especially considering the very similar microstructures of similarly fabricated specimens, which differed only in the kind of rare-earth element used. A more likely explanation for the observed contrast between neodynium and gadolinium compositions, we suggest, lies in the different solubility of their M′ solid solutions. As noted previously, M′(Nd) has the highest content of Al—O, hence the lowest content of Al—O in β′ and in the liquid. This could give the highest β′ strength after HP, but it also could give the poorest relative sintered density and, hence, the highest flaw population and lowest overall strength after GPS. On the other hand, M′(Gd) had the lowest content of Al—O, hence the highest content of Al—O in β′ and in the liquid. This could give the lowest β′ strength after HP but also the highest relative sintered density and, hence, the highest overall strength after GPS. The above reasoning is consistent with the density and composition data shown in Table V, as previously discussed in Section (III)(*1*)(*C*).

(3) Oxidation

Several samples in the α′–β′–M′ series were evaluated for oxidation resistance. The data of weight gain after oxidation in air for 20 h are shown in Fig. 9 as a function of temperature. Good oxidation resistance was found in all samples up to 1200°C, and no disintegration was seen up to 1400°C. Although no simple correlation of these data with the composition could be found, it does seem, however, that the oxidation resistance improves primarily with less M′ and secondarily with more β′.

IV. Conclusions

(1) Rare-earth melilite solid solution can be incorporated as a sintering aid in SiAlON formulations. Heated above the melting point of M′(R), ~1700°–1800°C, good sinterability is obtained for a variety of SiAlON composites with either α′ or β′ majority phase. For compositions without Al_2O_3 in the starting powders, M′(R) addition also yields high-density bodies after gas pressure sintering. These composites can withstand oxidation in air at 1200°C with relatively low weight gains.

(2) Distribution of M′(R) in the as-sintered state is dependent on the phase assemblage, the composition, and probably temperature. At higher oxide concentrations and in an α′-SiAlON-rich phase assemblage, larger liquid pockets of a size comparable to the grain size remain after sintering. At lower oxide concentrations and in a β′-SiAlON-rich phase assemblage, liquid is distributed initially and uniformly as a grain-boundary phase but later accumulates into large pockets as it crystallizes during annealing at lower temperatures. Crystallization of M′(R) with concurrent dissolution and solute redistribution of the majority SiAlON phases apparently occurs during postsintering annealing. However, a massive α′-to-β′ conversion with an attendant large increase of M′(R) apparently does not occur in our experiments.

(3) Sinterability at low concentrations of oxides is sensitive to the rare-earth elements used. This can be rationalized by the different Al—O solubility in M′(R). A lower solubility, as in M′(Gd), leaves a melt of a higher Al—O content, thus favoring sintering. La_2O_3 addition facilitates sintering without affecting equilibrium phase assemblage in these composites.

(4) Higher hardness but lower toughness are found for α′-rich composites and vice versa for β′- and polytypoid-rich composites. This is due to the inherently higher yield stress in α′ and the toughening of elongated β′ and polytypoid grains. Strength and toughness also are significantly higher in Al_2O_3-free compositions, because of a lower Al—O content in the β′-SiAlON. Overall, the most-promising properties have been obtained for the Al_2O_3-free compositions containing mostly β_9, with strength of 800–1000 MPa at room temperature and 500–600 MPa at 1200°C, toughness of 7 MPa·$m^{1/2}$ at room temperature, and hardness of 16 GPa.

References

[1]W. Y. Sun, P. A. Walls, and D. P. Thompson, "Reaction Sequences in Preparation of Sialon Ceramics"; pp. 105–17 in *Non-Oxide Technical and Engineering Ceramics, Proceedings of International Conference* (Limerick, Ireland, 1985). Edited by S. Hampshire. Elsevier, London, U.K., 1986.

[2]S. Slasor and D. P. Thompson, "Preparation and Characterization of Yttrium α′-SiAlONs"; see Ref. 1, pp. 223–30.

[3]S. Hampshire, K. P. J. O'Reilly, M. Leigh, and M. Redington, "Formation of α′-SiAlONs with Neodymium and Samarium Modifying Cations"; pp. 933–40 in *High Tech Ceramics*. Edited by P. Vincenzini. Elsevier, Amsterdam, The Netherlands, 1987.

[4]K. P. J. O'Reilly, M. Redington, S. Hampshire, and M. Leigh, "Parameters Affecting Pressureless Sintering of α′-SiAlONs with Lanthanide Modifying Cations"; pp. 393–98 in *Silicon Nitride Ceramics Scientific and Technological Advances*, Proceedings of Materials Research Society Symposium, Vol. 287 (Boston, MA, Nov. 30–Dec. 3, 1992). Edited by I-W. Chen, P. F. Becher, M. Mitomo, G. Petzow, and T. S. Yen. Materials Research Society, Pittsburgh, PA, 1993.

[5]P. O. Käll and T. Ekström, "Sialon Ceramics Made with Mixtures of Y_2O_3–Nd_2O_3 as Sintering Aids," *J. Eur. Ceram. Soc.*, **6**, 119–27 (1990).

[6]G. Z. Cao, R. Metselaar, and G. Ziegler, "Formation and Densification of α-Sialon Ceramics"; pp. 1285–93 in *Ceramics Today—Tomorrow's Ceramics*. Edited by P. Vincenzini. Elsevier, Amsterdam, The Netherlands, 1991.

[7]M. Redington and S. Hampshire, "Multi-Cation α-Sialon," *Br. Ceram. Proc.*, **49**, 175–90 (1992).

[8]P. L. Wang, W. Y. Sun, and T. S. Yen, "Sintering and Formation Behavior of R-α-Sialon (R = Nd, Sm, Gd, Dy, Er, and Yb)," *Eur. J. Solid State Inorg. Chem.*, **31** [93] 104 (1994).

[9]Y. B. Cheng and D. P. Thompson, "Preparation and Grain Boundary Devitrification of Samarium α-Sialon Ceramics," *J. Eur. Ceram. Soc.*, **14**, 13–21 (1994).

[10]M. Menon and I-W. Chen, "Reaction Densification of α′-SiAlON: I, Wetting Behavior and Acid–Base Reactions," *J. Am. Ceram. Soc.*, **78** [3] 545–52 (1995).

[11]M. Menon and I-W. Chen, "Reaction Densification of α′-SiAlON: II, Densification Behavior," *J. Am. Ceram. Soc.*, **78** [3] 553–59 (1995).

[12]Z. K. Huang and I-W. Chen, "Rare-Earth Melilite Solid Solution and Its Phase Relations with Neighboring Phases," *J. Am. Ceram. Soc.*, **79** [8] 2091–97 (1996).

[13]Y. Ukyo and S. Wada, "High-Strength Si_3N_4 Ceramics," *Nippon Seramikkusu Kyokai Gakujutsu Ronbunshi*, **97** [8] 872–74 (1989).

[14]T. S. Sheu, "Microstructure and Mechanical Properties of the *In Situ* β-Si_3N_4/α′-SiAlON Composite," *J. Am. Ceram. Soc.*, **77** [9] 2345–53 (1994).

[15]G. R. Anstis, P. Chantikul, B. R. Lawn, and D. B. Marshall, "A Critical Evaluation of Indentation Techniques for Measuring Fracture Toughness: I. Direct Crack Measurements," *J. Am. Ceram. Soc.*, **64** [9] 533–38 (1981).

[16]H. Mandal, D. P. Thompson, and T. Ekström, "Reversible α↔β Sialon Transformation in Heat-Treated Sialon Ceramics," *J. Eur. Ceram. Soc.*, **12**, 421–29 (1993).

[17]Z. J. Shen, T. Ekström, and M. Nygren, "Temperature Stability of Samarium-Doped α-SiAlON Ceramics," *J. Eur. Ceram. Soc.*, **16** [1] 43–53 (1996).

[18]H. R. Zhang, W. L. Li, J. W. Feng, Z. K. Huang, and D. S. Yan, "Si_3N_4–AlN Polytypoid Composites by GPS," *J. Eur. Ceram. Soc.*, **7**, 329–33 (1991).

[19]S. Tanabe, K. Hirao, and N. Soga, "Elastic Properties and Molar Volume of Rare-Earth Aluminosilicate Glasses," *J. Am. Ceram. Soc.*, **75** [3] 503–506 (1992).

[20]T. Ekström and M. Nygren, "SiAlON Ceramics," *J. Am. Ceram. Soc.*, **75** [2] 259–76 (1992).

[21]G. Z. Cao and R. Metselaar, "α′-SiAlON Ceramics: A Review," *Chem. Mater.*, **3**, 242–52 (1991).

[22]S.-L. Hwang and I-W. Chen, "Nucleation and Growth of α′-SiAlON on α-Si_3N_4," *J. Am. Ceram. Soc.*, **77** [7] 1711–18 (1994).

[23]W. D. Kingery, H. K. Bowen, and D. R. Uhlmann, *Introduction to Ceramics*, 2nd Ed. Wiley, New York, 1976.

[24]P. F. Becher, H. T. Lin, S. L. Hwang, M. J. Hoffmann, and I-W. Chen, "The Influence of Microstructure on the Mechanical Behavior of Silicon Nitride Ceramics"; pp. 147–58 in *Silicon Nitride Ceramics, Scientific and Technological Advances*. Materials Research Society Symposium Proceedings, Vol. 287. Edited by I-W. Chen, P. F. Becher, M. Mitomo, G. Petzow, and T.-S. Yen. Materials Research Society, Pittsburgh, PA, 1993. □